Proceedings of IMECE2004
2004 ASME International Mechanical Engineering Congress
Anaheim, California, USA, November 13-19, 2004

IMECE2004-59796

ULTRA-SHORT PULSED LASER TRANSPORT IN A MULTILAYERED TURBID MEDIA

Kamal M. Katika and Laurent Pilon*

Department of Mechanical and Aerospace Engineering
University of California
Los Angeles, California 90025
Email: pilon@seas.ucla.edu

ABSTRACT

This paper presents the modified method of characteristics for simulating the transient transport of light in an absorbing and scattering medium exposed to collimated light. This method is based on the method of characteristics that follows photons along their pathlines. After showing the validity of the method it is used to solve for the transient transport of light in human skin. Skin has been modelled as a seven layer medium with different scattering and absorbing coefficients and scattering asymmetry factors. The angular distribution of reflected light from skin is presented. This technique could be used as a tool for designing various biomedical applications.

NOMENCLATURE

c speed of light in the medium.
g scattering asymmetry factor.
I radiation intensity.
I_b blackbody radiation intensity.
I_c collimated radiation intensity.
I_d diffuse radiation intensity.
L thickness.
n refractive index.
R hemispherical reflectance
$\mathbf{r}$ position vector.
$\mathbf{r_w}$ position vector of a point on the boundary.
s geometric path length.
$\hat{\mathbf{s}}$ unit vector into a given direction.
T hemispherical transmittance
t time.
t_c pulse peak time.
t_p pulse width.
x, y, z Cartesian coordinates.
β extinction coefficient.
θ polar angle.
κ absorption coefficient.
λ wavelength.
μ direction cosine. ($\mu = \cos\theta$)
σ Stefan-Boltzman constant.
σ_s Scattering coefficient.
τ optical distance.
ϕ azimuthal angle.
Φ scattering phase function.
ω scattering albedo.
Ω solid angle.

INTRODUCTION

Traditional analysis of thermal radiation neglect the transient effect of light propagation, due to the large speed of light compared to the local time and length scales [1]. Of late, with the advent of ultra-short pulsed lasers this assumption is no longer valid. Ultrafast lasers are used in a wide variety of applications such as thin film property measurements, laser assisted micro-machining, laser removal of contamination particles from sur-

*Address all correspondence to this author.

faces, optical data storage, optical ablation and ablation of polymers [2].

Short-pulse lasers are also used in remote sensing of the atmosphere, combustion chambers and other environments which involve interaction of the laser beam with scattering and absorbing particles of different sizes. Particle size distributions and their optical properties can be reconstructed from measuring transmitted and reflected signals from short-pulse lasers [2].

Another interesting application of short-pulse lasers is in biomedical optical tomography where their use can potentially provide physiological and morphological information about the interior of living tissues and organs in a non-intrusive manner. Optical imaging using infrared radiation can also be used for other applications such as real time non-invasive monitoring of cryopreservation [2] and inspection of meat products for example [2]. Yamada *et al.* [3] have described a technique to compute the properties of a tissue based on temporal intensity measurements and an inverse method in order to determine the health of the tissue. The complexity is further increased by the difficulty to model radiative properties of tissue and their spatial variation.

Various methods have been developed to simulate transient radiation transport in absorbing and scattering media. The Monte-Carlo method is often used to simulate such problems because of its simplicity, the ease by which it can be applied to arbitrary configurations and its ability to capture real physical conditions [4]. However, it has inherent statistical errors due to its stochastic nature [1]. It is also computationally time consuming and demands a lot of computer memory as the histories of the photons have to be stored at every instant of time [4]. Thus, the Monte-Carlo method is ruled out in practical utilizations such as real-time clinical diagnostics where computational efficiency and accuracy are major concerns [5]. The backward or reverse Monte Carlo has been developed as an alternative approach when solutions are needed at particular locations and times [6, 7]. The method is similar to the traditional Monte Carlo method, except that the photons are tracked in a time-reversal manner. The photon bundles are traced from the detector to the source rather than from the source to the detector as in the conventional Monte Carlo method. There is no need to keep track of photons which do not reach the detector and so the reverse Monte Carlo method is much faster than the traditional Monte Carlo method. The method was successfully applied by Lu *et al.* [7] to simulate transient radiative transport in a non-emitting, absorbing, and anisotropically scattering one-dimensional slab subjected to ultra-short light pulse irradiation.

Other techniques include the integral equation solution [8–11], the discrete ordinates method in 2-D [12, 13] and 3-D [14], the finite volume method [15, 16], the radiation element method [5] and the diffusion approximation [17, 18]. The diffusion approximation has been extensively used in biomedical applications in order to simplify the radiative transfer problem. However, its validity for transient light transport in highly scattering media has been questioned [19]. Indeed, Elaloufi *et al.* [19] have shown that the diffusion approximation fails to describe both short-time and long-time radiation transport in thin slabs for both weakly and strongly absorbing cases. In the case of thick slabs, the diffusion approximation fails for short times. The authors have also shown that the diffusion theory always fails to predict the long-time behavior of transmitted pulses in thin slabs whose optical depth defined by $\tau_L = \sigma_s(1-g)L$ is less than eight.

Recently, the modified method of characteristics has been developed as an accurate technique to solve the equation for phonon radiative transfer (EPRT) [20]. The method was extended to solve the radiative transfer equation (RTE) for both steady and transient problems in homogeneous media with diffuse surfaces and incident intensities [21]. In this paper we extend the method further to solve the transient radiative transfer equation for a medium irradiated by a collimated ultra-short pulse laser beam. Then, it is used to simulate transient light transport in skin modelled as a multilayered turbid medium.

METHOD OF SOLUTION

The governing equation for radiative heat transfer is the radiative transfer equation. It is an energy balance on the radiative energy in the direction $\hat{\mathbf{s}}$ within a small pencil of rays. The change in intensity at any location in space is found by summing up the contributions from emission, absorption, scattering away from the direction $\hat{\mathbf{s}}$, and into the direction of $\hat{\mathbf{s}}$. It can be written as [1],

$$\frac{1}{c}\frac{\partial I_\lambda(\mathbf{r},\hat{\mathbf{s}},t)}{\partial t} + \hat{\mathbf{s}}\cdot\nabla I_\lambda(\mathbf{r},\hat{\mathbf{s}},t) = \kappa_\lambda(\mathbf{r})I_{b\lambda}(\mathbf{r},\hat{\mathbf{s}},t) - \kappa_\lambda(\mathbf{r})I_\lambda(\mathbf{r},\hat{\mathbf{s}},t) - \sigma_{s\lambda}(\mathbf{r})I_\lambda(\mathbf{r},\hat{\mathbf{s}},t) + \frac{\sigma_{s\lambda}(\mathbf{r})}{4\pi}\int_{4\pi} I_\lambda(\mathbf{r},\hat{\mathbf{s}}_i,t)\Phi_\lambda(\hat{\mathbf{s}}_i,\hat{\mathbf{s}})\mathrm{d}\Omega_i \quad (1)$$

where κ_λ and $\sigma_{s\lambda}$ are the linear absorption and linear scattering coefficients, respectively. I_λ and c are the intensity in the $\hat{\mathbf{s}}$ direction and the speed of light in the medium, respectively. The scattering phase function $\Phi_\lambda(\hat{\mathbf{s}}_i,\hat{\mathbf{s}})$ represents the probability that radiation propagating in direction $\hat{\mathbf{s}}_i$ be scattered into the cone $\mathrm{d}\Omega$ around the direction $\hat{\mathbf{s}}$. The first term on the right hand side represents the contribution from emission in the $\hat{\mathbf{s}}$ direction. The second and third terms represent attenuation by absorption and scattering, respectively. Finally, the last term represents the augmentation of radiation due to in-scattering.

To solve the radiative transport equation for collimated irradiation, the intensity is split into two parts, (i) the radiation scattered away from the collimated radiation and (ii) the remaining collimated beam after partial extinction by absorption and scattering along its path. The contribution from emission is usually negligible compared to the incident and scattered intensity. Thus,

the intensity for a gray medium is written as

$$I(\mathbf{r},\hat{\mathbf{s}},t) = I_c(\mathbf{r},\hat{\mathbf{s}},t) + I_d(\mathbf{r},\hat{\mathbf{s}},t) \tag{2}$$

The collimated remnant of the incident irradiation $I_i(\mathbf{r}_w,t)$ obeys the equation of transfer

$$\frac{1}{c}\frac{\partial I_c(\mathbf{r},\hat{\mathbf{s}},t)}{\partial t} + \hat{\mathbf{s}}\cdot\nabla I_c(\mathbf{r},\hat{\mathbf{s}},t) = -\beta I_c(\mathbf{r},\hat{\mathbf{s}},t) \tag{3}$$

subject to the boundary condition

$$I_c(\mathbf{r}_w,\hat{\mathbf{s}},t) = I_i(\mathbf{r}_w,t)\delta[\hat{\mathbf{s}}-\hat{\mathbf{s}}_c(\mathbf{r}_w)] \tag{4}$$

The solution of these equations is given by [22]

$$I_c(\mathbf{r},\hat{\mathbf{s}},t) = I_i(\mathbf{r}_w,t-s/c)\delta[\hat{\mathbf{s}}-\hat{\mathbf{s}}_c(\mathbf{r}_w)]\times \exp\left[-\int_0^s \beta(\mathbf{r}-s'\hat{\mathbf{s}})ds'\right] H(t-s/c) \tag{5}$$

where $s = |\mathbf{r}-\mathbf{r}_w|$ and H is the Heaviside step function ($H(u) = 0$ if $u < 0$ and $H(u) = 1$ if $u \geq 0$). Substituting Equations (2) and (3) into Equation (1) for a gray medium gives the governing equation for the noncollimated radiation intensity I_d,

$$\frac{1}{c}\frac{\partial I_d(\mathbf{r},\hat{\mathbf{s}},t)}{\partial t} + \hat{\mathbf{s}}\cdot\nabla I_d(\mathbf{r},\hat{\mathbf{s}},t) = -\beta(\mathbf{r})I_d(\mathbf{r},\hat{\mathbf{s}},t) + \kappa(\mathbf{r})I_b(\mathbf{r},\hat{\mathbf{s}},t) + \frac{\sigma_s(\mathbf{r})}{4\pi}\int_{4\pi} I_d(\mathbf{r},\hat{\mathbf{s}}_i,t)\Phi(\hat{\mathbf{s}}_i,\hat{\mathbf{s}})\mathrm{d}\Omega_i + \sigma_s(\mathbf{r})S_c(\mathbf{r},\hat{\mathbf{s}},t) \tag{6}$$

where

$$S_c(\mathbf{r},\hat{\mathbf{s}},t) = \frac{1}{4\pi}\int_{4\pi} I_c(\mathbf{r},\hat{\mathbf{s}}_i,t)\Phi(\hat{\mathbf{s}}_i,\hat{\mathbf{s}})\mathrm{d}\Omega_i \tag{7}$$

Note that Equations (3) and (6) sum up to give Equation (1).

MODIFIED METHOD OF CHARACTERISTICS

The method of characteristics consists of transforming the radiative transport equation, an integro-differential equation into an ordinary differential equation along the photon pathlines. The advantages and disadvantages of the modified method of characteristics have been summarized by Pilon and co-workers and need not be repeated here [23–25]. Consider a Cartesian coordinate system, the characteristic in physical space is defined as

$$\frac{\mathrm{d}x}{\mathrm{d}t} = c\sin\theta\cos\phi \tag{8}$$

$$\frac{\mathrm{d}y}{\mathrm{d}t} = c\sin\theta\sin\phi \tag{9}$$

$$\frac{\mathrm{d}z}{\mathrm{d}t} = c\cos\theta \tag{10}$$

By definition, the total derivative $\mathrm{D}/\mathrm{D}t$ can be written as

$$\frac{\mathrm{D}}{\mathrm{D}t} = \frac{\partial}{\partial t} + \frac{\mathrm{d}x}{\mathrm{d}t}\frac{\partial}{\partial x} + \frac{\mathrm{d}y}{\mathrm{d}t}\frac{\partial}{\partial y} + \frac{\mathrm{d}z}{\mathrm{d}t}\frac{\partial}{\partial z} \tag{11}$$

Then, along the characteristic curves in (x,y,z,t) space, Equation (6) simplifies to

$$\frac{1}{c}\frac{\mathrm{D}}{\mathrm{D}t}I_d(\mathbf{r},\hat{\mathbf{s}},t) = \kappa(\mathbf{r})I_b(\mathbf{r},\hat{\mathbf{s}},t) - \beta(\mathbf{r})I_d(\mathbf{r},\hat{\mathbf{s}},t) + \frac{\sigma_s(\mathbf{r})}{4\pi}\int_{4\pi} I_d(\mathbf{r},\hat{\mathbf{s}}_i,t)\Phi(\hat{\mathbf{s}}_i,\hat{\mathbf{s}})\mathrm{d}\Omega_i + \sigma_s(\mathbf{r})S_c(\mathbf{r},\hat{\mathbf{s}},t) \tag{12}$$

Thus, a partial differential equation is converted into three ordinary differential equations and one integro-differential equation in time. Figure 1 shows a 3-D computational cell in Cartesian coordinates. To solve Equations (8) to (12), the radiation intensities and temperatures are initialized at all points in the computational domain. Then, for a given polar angle θ_n, an azimuthal angle ϕ_l, and for all internal grid points (x_a, y_b, z_c) where photons are present at time $t+\Delta t$, the position of the photon at time t is calculated as

$$x_n = x_a - c\sin\theta_n\cos\phi_l\Delta t \tag{13}$$

$$y_n = y_b - c\sin\theta_n\sin\phi_l\Delta t \tag{14}$$

$$z_n = z_c - c\cos\theta_n\Delta t \tag{15}$$

The values of the variables I_λ at (x_n,y_n,z_n) and time t are obtained by Lagrangian interpolation using their values at time t at the eight corners of the computational cell in which (x_n,y_n,z_n) is located (Figure 1). Then, Equation (12) is solved by the fourth order Runge-Kutta method at location (x_a, y_b, z_c) and time $t+\Delta t$. The integral on the right hand side of Equation (12) is estimated by the 3/8 Simpson numerical integration. Finally, the boundary conditions are imposed. The calculations are repeated for all the discretized values of polar and azimuthal angles as well as discretized wavelengths in case of spectral calculations. The spectral dependencies can be accounted for by using the modified method of characteristics at multiple wavelengths or in combination with band models [1].

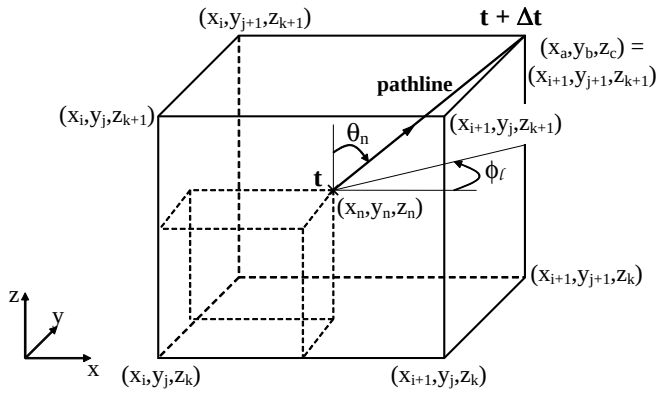

Figure 1. TYPICAL COMPUTATIONAL CELL USED FOR INVERSE MARCHING METHOD CONTAINING THE PATHLINE OF THE PHOTONS.

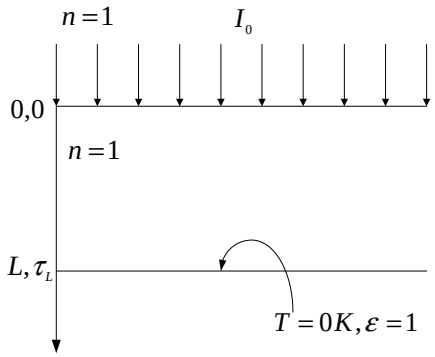

Figure 2. PARALLEL BLACK WALLS SEPARATED BY AN ABSORBING MEDIUM AND EMITTING MEDIUM.

RESULTS AND DISCUSSION

The problem of light transport in a multilayer slab of skin exposed to collimated laser light is considered. For validation purposes, transient light transport in a homogeneous slab was first simulated. The numerical results obtained with the modified method of characteristics were compared with the results reported by Wu [11]. For the sake of clarity, spectral dependencies were not considered in these cases.

Transient radiative transfer in a plane, parallel, non emitting, absorbing and isotropically scattering media

Consider a plane parallel slab of an absorbing and isotropically scattering medium with constant and uniform optical properties exposed to time-dependent collimated radiation as shown in Figure 2. In this case, Equation (5) simplifies to

$$I_c(z,\hat{\mathbf{s}},t) = I_i(t-z/c)\delta[\hat{\mathbf{s}}-\hat{\mathbf{s}}_c]e^{-\beta z} \tag{16}$$

where $\hat{\mathbf{s}}_c$ corresponds to $\cos\theta = 1$, while the incident radiation is a truncated Gaussian distribution with a peak intensity at $t = t_c$ and pulse width t_p expressed as

$$I_i(t) = I_0 \exp\left[-4\ln 2\left(\frac{t-t_c}{t_p}\right)^2\right], \qquad 0 < t < 2t_c \tag{17}$$

$$I_i(t) = 0, \qquad t \geq 2t_c \tag{18}$$

Moreover, the source term defined in Equation (7) simplifies to

$$S_c(z,t) = \frac{1}{4\pi} I_i(t-z/c)e^{-\beta z}H(t-z/c) \tag{19}$$

Equation (12) then becomes

$$\frac{1}{c}\frac{\mathrm{D}I_d(z,\hat{\mathbf{s}},t)}{\mathrm{D}t} = -\beta I_d(z,\hat{\mathbf{s}},t) + \frac{\sigma_s}{4\pi}\int_{4\pi} I_d(z,\hat{\mathbf{s}}_i,t)\mathrm{d}\Omega_i + \frac{\sigma_s}{4\pi} I_i(t-z/c)e^{-\beta z}H(t-z/c) \tag{20}$$

with $\hat{\mathbf{s}}$ dependent only on the polar angle θ, and the boundary conditions being $I_d(z=0,\cos\theta>0,t)=0$ and $I_d(z=L,\cos\theta<0,t)=0$.

To solve the problem using the modified method of characteristics, a spatial discretization of 101 points along the $z-$direction for the case of $\tau_L = 0.5$ and 201 points for the case of $\tau_L = 5.0$ is used. The mean change in the results obtained by using a discretization of 201 and 301 points for the two cases respectively was less than 1%. An angular discretization of 12×1 directions per octant is used. An angular discretization of 18×1 angles per octant resulted in a mean change of less than 1% in the reflectance. Thus, a converged solution in terms of both grid size and number of directions has been achieved. The time interval Δt had little effect on the numerical results as long as $\Delta t \leq \Delta z/c$. Thus, it was set equal to $\Delta z/c$ where $\Delta z = L/(N_z-1)$ and N_z is the number of gridpoints in the $z-$direction. After solving for the intensities in all directions at every grid point, the hemispherical reflectance and transmittance are computed using the following formulae :

$$R(t) = -2\pi\int_{-1}^{0} I_d(0,\mu,t)\mu\mathrm{d}\mu/I_0 \tag{21}$$

and

$$T(t) = [2\pi\int_0^1 I_d(L,\mu,t)\mu\mathrm{d}\mu + I_i(t-L/c)e^{-\beta L}H(t-L/c)]/I_0 \tag{22}$$

Figures 3 and 4 compare the transmittance and reflectance of two slabs computed by Wu [11] by solving the integral equation with those obtained with the modified method of characteristics. Good agreement is observed and the mean error was less than 5% in all cases. Thus, the present method can be used to reliably solve ultra-short pulse laser transport in turbid media including skin.

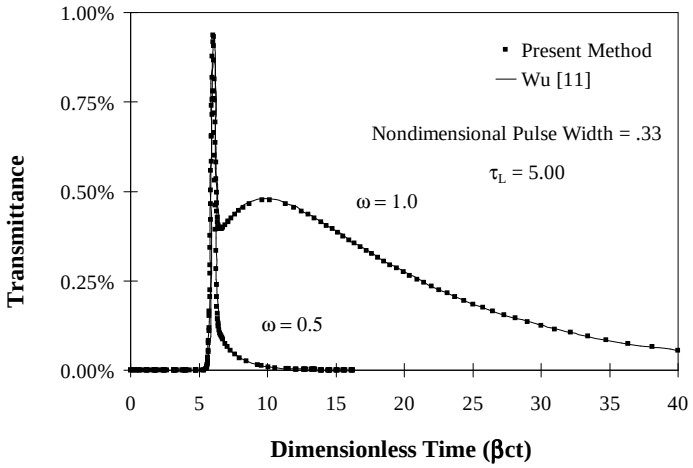

Figure 3. TIME-RESOLVED HEMISPHERICAL TRANSMITTANCE FOR $\tau_L = 5.0$, $t_c/t_p = 3$ and $\beta c t_p = 0.33$.

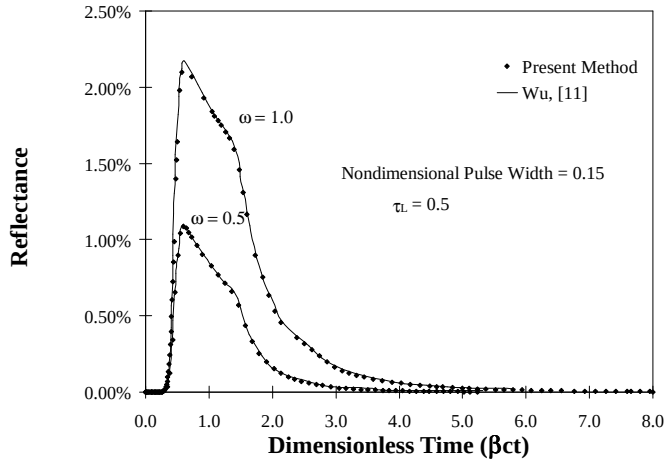

Figure 4. TIME-RESOLVED HEMISPHERICAL REFLECTANCE FOR $\tau_L = 0.5$, $t_c/t_p = 3$ and $\beta c t_p = 0.15$.

LIGHT TRANSPORT IN SKIN

Many therapeutic and diagnostic techniques in medicine depend on interactions of light with tissues. In most cases, radiation is incident on the surface of the tissue and the measured reflectance and transmittance provides information about the medium. Numerous models have been developed that predict the distribution of light in tissue. Radiative transport through skin plays a very important role in all these applications as light must first pass through the skin before it reaches other parts of the body. It is also important when skin is the site for photobiologic reactions to treat various disorders. Central to predicting radiative transport in skin is the development of a model which captures the various spatially varying properties of the skin. The major chromophores present in the skin are normally confined to distinct layers [26]. For example, melanin is usually confined to the epidermis and stratum corneum while hemoglobin is usually confined to the vessels of the dermis [26]. Thus, the skin can be modelled as a layered media each having different thickness and optical properties. The layers are assumed to have the same refractive index ($n = 1.4$) but different number density of absorbers and scatterers uniformly distributed in each layer [27]. The diffusion approximation with an equivalent isotropic scattering coefficient is commonly used to analyze problems involving light transport in tissue [28]. This approach, even though it can predict the transmittance and reflectance of highly turbid media, it cannot predict the shape of the angular profile of the reflected or transmitted intensities. Knowing the angular profile of the intensities could be valuable in designing optical devices for biomedical applications.

The modified method of characteristics can solve the complete radiative transfer equation without making any approximations. It can also predict the angular intensity profile at all locations in the domain. We have used the modified method of characteristics to model the transport of light through skin based on a model and optical properties successfully used by Zeng *et al.* [29] for reconstruction of the *in vivo* autofluorescence spectrum of skin. The authors modelled skin as a seven layered structure whose thickness and optical properties at wavelength 442 *nm* are reproduced in Table 1. The total thickness of the skin model was 2 *mm*. The skin is in contact with a medium matching its refractive index in which the source and the detectors are submerged. If the skin sample were exposed to air, then the mismatch in refractive index would have to be taken into account. Indeed, a photon that reaches the air-skin interface at an angle greater than the critical angle defined by $\theta_c = \arcsin(1/n)$ where *n* is the refractive index of the medium, would be reflected back into the tissue. The critical angle for the air-skin interface is 41.8° [27]. In spite of varying refractive indices within the skin, reflection and refraction effects at the interfaces were not taken into account as the change in the refractive index was very minimal. Instead, only the speed of light, $c = c_0/n$, was varied in each layer based on the refractive index. Had there been a

larger change in the refractive indices at the interfaces, then the RTE would have had to be solved in each layer separately. At the interfaces, various boundary conditions can be used based on whether the interface is optically smooth, partially diffuse or specular. For example, if it were optically smooth and specular, the rays would be reflected and refracted according to Snell's laws and the transmitted and reflected intensities computed using Fresnel's equations [1].

The Henyey-Greenstein phase function was used to account for the anisotropic nature of scattering by the tissue and is expressed as

$$\Phi(\Theta) = \frac{1-g^2}{[1+g^2-2g\cos\Theta]^{3/2}} \tag{23}$$

where, g is the asymmetry factor. A plot of the Henyey-Greenstein phase function for $g = 0.9$ and $g = 0.75$ corresponding to the stratum-corneum and top layers of the dermis is shown in Figure 5. One can see that all layers of the skin are strongly forward-scattering, particularly the stratum-corneum. Figure 6 shows the profile of the back scattered radiation for the same values of g.

A grid was generated such that the interfaces between the skin layers fell on grid points. A discretization of 10 gridpoints in each layer and 12×1 angles per octant was used. In a second test, a discretization of 20 gridpoints in each layer and 12×1 angles per octant was also used. The mean difference in the computed reflectance was about 2% and the solution was considered to be converged in terms for 10 grid points per layer. Two other tests, both with a discretization of 10 gridpoints in each layer but one with 30×1 angles per octant and another with 36×1 angles per octant were performed. The mean difference in the computed reflectances was less than 1.5% and the solution was considered to be converged in terms of directions for 30×1 angles per octant.

Figure 7 shows the angular profile of the reflected light at various times. The peak of the reflectance occurs around 6.5ps and so the angular reflectivity was plotted at this times and other times where it reaches half and one quarter of its maximum value. The angular profile of the reflected intensity changes with time and becomes more forward scattering as time progresses. This can be attributed to the fact that the major contribution to the reflectance is initially due to photons which have been backscattered by the topmost layers of the tissue and have not undergone many scattering events. Therefore the directional profile of the reflected intensity at earlier times resembles the backscattering profile for $g = 0.9$ shown in Figure 6.

On the other hand, photons which arrive long after the incident pulse has died down (at $t = 9ps$, it is about 0.2% of its peak intensity), are those which have undergone multiple scattering events in the tissue and so the angular profile of the intensities

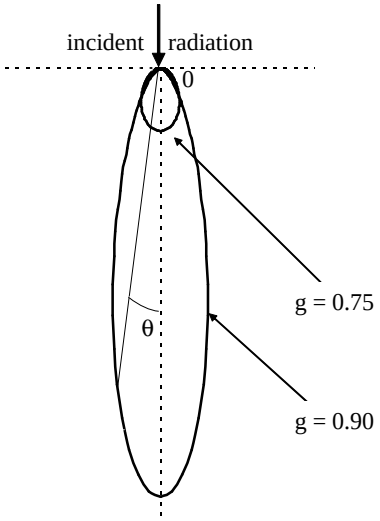

Figure 5. THE HENYEY-GREENSTEIN FUNCTION FOR $g = 0.9$ AND $g = 0.75$.

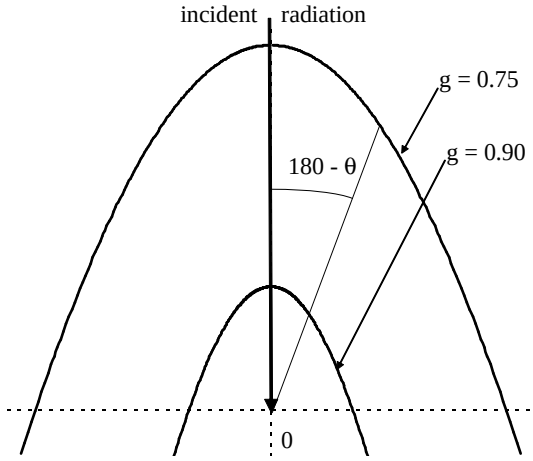

Figure 6. PROFILE OF THE BACKSCATTERED RADIATION USING THE HENYEY-GREENSTEIN PHASE FUNCTION FOR $g = 0.9$ AND $g = 0.75$ for $\pi/2 \leq \theta \leq \pi$.

closely resembles a strongly forward scattering medium shown in Figure 5.

Further simulations were carried out to test the influence of the scattering asymmetry factor g in various layers of the tissue on the reflected signal. Figure 8 shows the hemispherical reflectance as a function of time for a pulse width of 2 picoseconds for a discretization of 10 grid points in each layer and 30×1 an-

gles per octant. The scattering asymmetry factor g was changed to -0.5 in the upper blood plexus, the dermis and the lower blood plexus. Practically, g can be varied in tissue by various means such as injection of microbbubles or microspheres into the blood stream to increase backscattering [30, 31]. A cream containing back scattering particles (typically nano- or micro-particles) can also be applied onto the skin. It was seen that changing the asymmetry factor (to g = -0.5) in the lower layers of the tissue rich in blood vessels, namely the blood plexus, does not result in a significant change in the reflectance. At the wavelength of 442 nm, only changes in the topmost layers are detectable in the measured reflectance. Figure 8 compares the reflectance of the skin in which the stratum corneum is strongly backscattering ($g = -0.9$) with that of normal skin.

In general, the scattering properties of the skin are directly related to the cells and their internal structure [32]. This could be used in tissue diagnostics. For example, Maier *et al.* [33] have proposed a possible correlation between blood glucose concentration and the reduced scattering coefficient of the tissue. Light scattering occurs in tissues because of the mismatch of index of refraction between the extracellular fluid (ECF) and the membranes of the cells composing the tissue [33]. The refractive index of ECF changes as a function of glucose concentration and so any change in the glucose concentration can be detected by observing the changes in the reflectance.

CONCLUSION

The modified method of characteristics has been extended to solve transport of a collimated ultra-short pulse laser beam in highly scattering media. Good agreement has been observed with reported results for the same case obtained by Wu [11] by solving the integral equation. Then, the method has been used to solve for the light transport in human skin modelled as a seven layer medium. The angular variation of light reflected from skin has been presented. Even though only 1-D geometries and simple boundary conditions were considered, this method can be easily extended to handle more complex geometries and boundary conditions. This could be a potential design tool for various biomedical applications ranging from optimal placement of light sources and detectors for tomographic applications to design of advanced sunscreens. Since this method is fully explicit, it can be easily adapted for parallel computing. This would be valuable in various applications, such as real time tomographic analysis, where this technique along with an inverse method could be used to detect tumors and other malignancies in the human body.

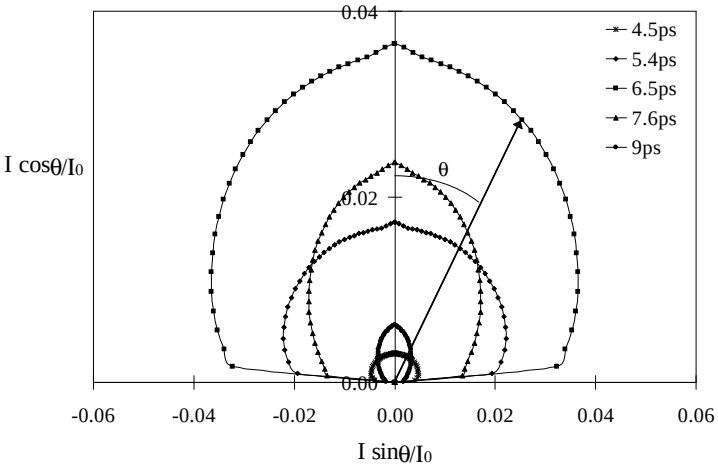

Figure 7. ANGULAR PROFILE OF REFLECTED INTENSITY AT VARIOUS TIMES.

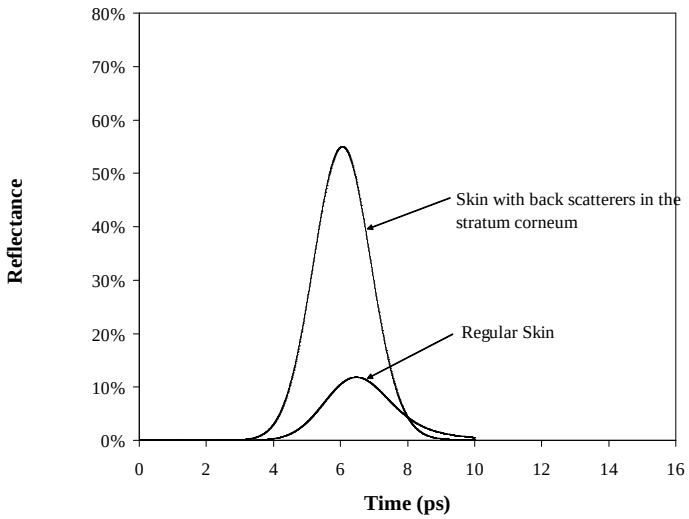

Figure 8. TIME-RESOLVED HEMISPHERICAL REFLECTANCE FOR A SLAB OF SKIN.

REFERENCES

[1] Modest, M. F., 2003. *Radiative Heat Transfer*. McGraw-Hill, New York, NY.

[2] Kumar, S., and Mitra, K., 1999. "Microscale aspects of thermal radiation transport and laser applications". *Advances in Heat Transfer,* **33** , pp. 187–294.

[3] Yamada, Y., 1995. "Light-tissue interaction and optical imaging in biomedicine". Annual Review of Heat Transfer, **6** (2) , pp. 1–59.

[4] Guo, Z., Kumar, S., and San, K.-C., 2000. "Multidimensional Monte Carlo simulation of short-pulse transport in scattering media". Journal of Thermophysics and Heat Transfer, **14** (4) , pp. 504–511.

Table 1. THE SEVEN-LAYER OPTICAL MODEL. THE PROPERTIES ARE FOR 442 nm.

Layer	d (μm)	n	σ_s (cm^{-1})	μ_a (cm^{-1})	g
Air	–	1.0	–	–	–
Stratum Corneum	10	1.45	190	2300	0.9
Epidermis	80	1.4	56	570	0.75
Papillary dermis	100	1.4	6.7	700	0.75
Upper blood plexus	80	1.39	67	680	0.77
Reticular dermis	1500	1.4	6.7	700	0.75
Deep blood plexus	70	1.34	541	520	0.96
Dermis	160	1.4	6.7	700	0.75
Subcutaneous fat	–	1.46	–	–	–

[5] Guo, Z., and Kumar, S., 2001. "Radiation element method for transient hyperbolic radiative transfer in plane parallel inhomogenous media". Numerical Heat Transfer,Part B, **39** (4) , pp. 371–387.

[6] Modest, M. F., 2003. "Backward Monte Carlo simulations in radiative heat transfer". ASME Journal of Heat Transfer, **125** (1) , pp. 57–62.

[7] Lu, X., and Hsu, P.-F., 2003. "Reverse Monte Carlo method for transient radiative transfer in participating media". *Proceedings of the ASME International Mechanical Engineering Congress and Exposition* .

[8] Tan, Z.-M., and Hsu, P.-F., 2001. "An integral formulation of transient radiative transfer". ASME Journal of Heat Transfer, **123** (3) , pp. 466–475.

[9] Wu, C.-Y., and Wu, S.-H., 2000. "Integral equation formulation for transient radiative transfer in an anisotropically scattering medium". International Journal of Heat and Mass Transfer, **43** (11) , pp. 2009–2020.

[10] Tan, Z.-M., and Hsu, P.-F., 2002. "Transient radiative transfer in three-dimensional homogeneous and non-homogeneous participating media". Journal of Quantitative Spectroscopy and Radiative Transfer, **73** (2) , pp. 181–194.

[11] Wu, C.-Y., 2000. "Propagation of scattered radiation in a participating planar medium with pulse irradiation". Journal of Quantitative Spectroscopy and Radiative Transfer, **64** (5) , pp. 537–548.

[12] Sakami, M., Mitra, K., and Hsu, P.-F., 2002. "Analysis of light pulse transport through two-dimensional scattering and absorbing media". Journal of Quantitative Spectroscopy and Radiative Transfer, **73** (2) , pp. 169–179.

[13] Guo, Z., and Kumar, S., 2001. "Discrete ordinates solution of short pulse laser transport in two-dimensional turbid media". Applied Optics, **40** (19) , pp. 3156–3163.

[14] Guo, Z., and Kumar, S., 2002. "Three-dimensional discrete ordinates method in transient radiative transfer". Journal of Thermophysics and Heat Transfer, **16** (3) , pp. 289–296.

[15] Chai, J., 2003. "One-dimensional transient radiation heat transfer modeling using a finite-volume method". Numerical Heat Transfer, Part B, **44** (2) , pp. 187–208.

[16] Chai, J. C., Hsu, P.-F., and Lam, Y., 2004. "Three-dimensional transient radiative transfer modeling using the finite-volume method". Journal of Quantitative Spectroscopy and Radiative Transfer, **86** (3) , pp. 299–313.

[17] Ishimaru, A., 1989. "Diffusion of light in turbid material". Applied Optics, **28** (12) , pp. 2210–2215.

[18] Patterson, M., Chance, B., and Wilson, B., 1989. "Time resolved reflectance and transmittance for the non-invasive measurement of tissue optical properties". Applied Optics, **28** (12) , pp. 2331–2336.

[19] Elaloufi, R., Carminati, R., and Greffet, J. J., 2002. "Time-dependent transport through scattering media: from radiative transfer to diffusion". Journal of Optics A: Pure And Applied Optics, **4** (5) , pp. S103–S108.

[20] Pilon, L., and Katika, K., 2004. "Backward method of characteristics for simulating microscale energy transport,". ASME Journal of Heat Transfer, to appear, **126** (4) .

[21] Katika, K., and Pilon, L., 2004. "Backward method of characteristics in radiative heat transfer". *4th International Symposium on Radiative Transfer, June 20-25, Istanbul* , pp. 347–355.

[22] Pomraning, G. C., 1973. *The Equations of Radiation Hydrodynamics*. Pergamon Press, New York, NY.

[23] Pilon, L., and Viskanta, R., 2003. "Modified method of characteristics for solving the population balance equation". International Journal for Numerical Methods in Fluids, **42** (11) , pp. 1211–1236.

[24] Pilon, L., Fedorov, A. G., Ramkrishna, D., and Viskanta, R., 2004. "Bubble transport in three-dimensional gravity driven flow, part i. mathematical formulation". *Journal of Non-Crystalline Solids*, **336** , pp. 71–83.

[25] Pilon, L., and Viskanta, R., 2004. "Bubble transport in three-dimensional gravity driven flow, part ii. numerical results". *Journal of Non-Crystalline Solids*, **336** , pp. 84–95.

[26] Anderson, R., and Parrish, J., 1981. "The optics of human skin". Journal of Investigative Dermatology, **77** (1) , pp. 13–19.

[27] Gemert, M. J. C. V., Jacques, S. L., Sterenborg, H. J. C. M., and Star, W. M., 1989. "Skin optics". IEEE Transactions on Biomedical Engineering, **36** (12) , pp. 1146–1154.

[28] Yamada, Y., 2000. "Fundamental studies of photon migration in biological tissues and their application to optical tomography". Optical Review, **7** (5) , pp. 366–374.

[29] Zeng, H., MacAulay, C., McLean, D. I., and Palcic, B., 1997. "Reconstruction of in vivo skin autofluorescence

spectrum from microscopic properties by Monte Carlo simulation". Journal of Photochemistry and Photobiology B: Biology, **38** (3) , pp. 234–240.

[30] Barton, J. K., Hoying, J. B., and Sullivan, C. J., 2002. "Use of microbubbles as an optical coherence tomography contrast agent". Academic Radiology, **9** (1) , pp. S52–S55.

[31] Lee, T. M., Oldenburg, A. L., Sitafalwalla, S., Marks, D. L., Luo, W., Toublan, F. J. J., Suslick, K. S., and Boppart, S. A., 2003. "Engineered microsphere contrast agents for optical coherence tomography". Optics Letters, **28** (17) , pp. 1546–1548.

[32] Mourant, J. R., Freyer, J. P., Hielscher, A. H., Eick, A. A., Shen, D., and Johnson, T. M., 1998. "Mechanisms of light scattering from biological cells relevant to noninvasive optical-tissue diagnostics". Applied Optics, **37** (16) , pp. 3586–3593.

[33] Maier, J. S., Walker, S. A., Fantini, S., Franceschini, M. A., and Gratton, E., 1994. "Possible correlation between blood glucose concentration and the reduced scattering coefficient of tissues in the near infrared". Optics Letters, **19** (24) , pp. 2062–2064.